



## Towards complete decay spectroscopy of $^{152}\text{Tb}$

E.B. O'Sullivan<sup>a,b</sup>, S.M. Collins<sup>a,b</sup>, J.-M. Daugas<sup>c</sup>, L. Domenichetti<sup>c</sup>, J. Heery<sup>a</sup>, J. Henderson<sup>a</sup>, U. Köster<sup>c</sup>, C. Michelagnoli<sup>c</sup>, T. Parry<sup>a,d</sup>, S. Pascu<sup>a,e</sup>, P.H. Regan<sup>a,b</sup>, R. Shearman<sup>b</sup>

<sup>a</sup> School of Mathematics and Physics, University of Surrey, Guildford, GU2 7XH, UK

<sup>b</sup> National Physical Laboratory, Hampton Road, Teddington, Middlesex, TW11 0LW, UK

<sup>c</sup> Institut Laue-Langevin, Grenoble, France

<sup>d</sup> Facility for Rare Isotope Beams, Michigan State University, East Lansing, MI 48824, USA

<sup>e</sup> National Institute for Physics and Nuclear Engineering, Bucharest-Magurele, R-77125, Romania

### ARTICLE INFO

#### Keywords:

Spectroscopy  
Nuclear medicine  
Radiation physics  
Medical imaging  
Beta decay  
Terbium-152

### ABSTRACT

The radionuclide  $^{152}\text{Tb}$ , decaying by  $\beta^+$  emission and electron capture to  $^{152}\text{Gd}$  with  $T_{1/2} = 17.8784(95)$  h, has been shown in its first-in-human use to be suitable for positron emission tomography (PET) imaging. As a member of the terbium theragnostic quartet, this radionuclide has potential applications in personalised cancer treatments. Sources of  $^{152}\text{Tb}$  were produced by proton-induced spallation of a tantalum target followed by on-line mass separation at CERN-ISOLDE. The sources were delivered to ILL Grenoble, where gamma–gamma coincidence spectroscopy of excited states populated in  $^{152}\text{Gd}$  following the decay was carried out using the Fission Product Prompt  $\gamma$ -ray Spectrometer (FIPPS). Preliminary analysis has resulted in the identification of multiple previously unreported excited states in  $^{152}\text{Gd}$ , thirteen of which are reported here at excitation energies up to 3746 keV. Angular correlation analysis has been used to provide initial spin and parity assignments to excited states. The result of the completed spectroscopy will be a revised gamma-ray and  $\beta^+$  dose to patients compared to the current expected values.

### 1. Introduction

Terbium-152 is a radionuclide with attractive properties for nuclear medicine. Decaying from the  $J^\pi = 2^-$  ground state by electron capture and  $\beta^+$  decay to  $^{152}\text{Gd}$ ,  $^{152}\text{Tb}$  is suitable for positron emission tomography (PET) imaging. The decay has  $T_{1/2} = 17.8784(95)$  h (Collins et al., 2023) and  $Q_{EC} = 3990(40)$  keV (Martin, 2013), and in-human trials have shown good performance in PET imaging of prostate cancer and neuroendocrine tumours in patients (Baum et al., 2017; Müller et al., 2019).

The terbium theragnostic quartet is a group of four terbium isotopes, each having different decay properties and therefore different medical uses. Comprising  $^{149,152,155,161}\text{Tb}$ , the quartet is a key avenue of research in the field of theragnostics, combining diagnostics and therapy into a unified treatment for cancer (Müller et al., 2018). Due to the shared chemical properties of isotopes of the same element, each member of the quartet is compatible with the same targeting molecules that deliver the radionuclide to the site of the tumour in the patient. This allows the uptake of the radiopharmaceutical (composed of the targeting molecule labelled with the radionuclide) to be measured using the imaging isotope, guiding the subsequent application of the therapeutic isotope using the same delivery vector. The treatment plan can therefore be

tuned to the requirements of each specific patient, making theragnostics a personalised approach to cancer treatment (Gomes Marin et al., 2020). It is the membership of this quartet that gives  $^{152}\text{Tb}$  its main advantage over traditional PET isotopes.

Quantification of the radioactive dose received by patients depends on accurate nuclear data, in particular the photon and charged particle spectra emitted in the decay. A comprehensive level scheme detailing gamma-ray energies and emission probabilities, as well as the beta feeding into each level, are therefore valuable in determining the patient dose.

The most recent evaluation of the nuclear data for the decay of  $^{152}\text{Tb}$  took place in 2013 (Martin, 2013), with the most recent published study taking place in 2003 using a pair of high purity germanium (HPGe) detectors to measure gamma–gamma coincidences (Adam et al., 2003). The highest identified energy state populated in the  $^{152}\text{Gd}$  daughter following the decay is at 3358 keV, more than 600 keV below the  $Q_{EC}$ . Furthermore, 248 out of the 635 transitions identified in this study remain unplaced on the level scheme (Nichols, 2022). Further excited states have been reported up to 3570 MeV in a 2014 PhD thesis based on gamma–gamma coincidence analysis, but these results have

\* Corresponding author at: School of Mathematics and Physics, University of Surrey, Guildford, GU2 7XH, UK.

E-mail address: [eo00268@surrey.ac.uk](mailto:eo00268@surrey.ac.uk) (E.B. O'Sullivan).

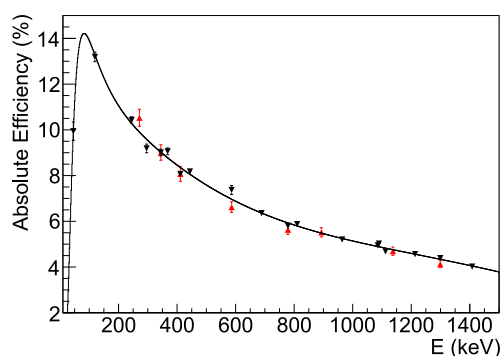


Fig. 1. Preliminary efficiency curve for FIPPS, fit to peaks in the decay of a  $^{152}\text{Eu}$  calibration source (black) using the coincidence counting method. Gamma rays emitted in the decay of  $^{152}\text{Tb}$  are shown in red for comparison.

not been confirmed in a peer-reviewed publication (Beller, 2014). A level density calculation reports over 400 states in the range 3–4 MeV that may be populated by allowed beta decays from  $^{152}\text{Tb}$ , suggesting that many further levels remain undetected (Capote et al., 2009).

At present, the evaluated nuclear data are likely to be limited by the pandemonium effect: the low efficiency of high-resolution gamma-ray detectors at high energies limits the detection of gamma rays depopulating high-energy excited states; in turn this limits knowledge of the low-energy beta decays populating these excited states (Hardy et al., 1977). As a consequence of the high density of states as the excitation energy increases, this leads to a significant low-energy beta emission component that is missing from the current evaluation of the decay. This systematic error can be partially mitigated with the use of higher efficiency detector arrays, supported by complementary experimental techniques such as total absorption gamma-ray spectroscopy (TAS) (Rubio et al., 2017).

Recent studies of similar  $\beta^+$ -decaying medical isotopes have revealed that decay schemes may be far more complex than previous measurements indicate. The identification of further gamma rays and energy levels has led to significant shifts in beta decay strength functions, and relative reductions in positron emission probabilities of over 10% in some cases (Gula et al., 2020; Nichols, 2022). A revisited spectroscopy of  $^{152}\text{Tb}$  with a higher efficiency array setup is likely to result in a similar shift in the beta decay strength function, and a subsequent revision of the beta dose.

## 2. Experiment

$^{152}\text{Tb}$  was produced at the ISOLDE facility at CERN, using a 1.4 GeV proton beam incident on a tantalum target. The spallation products diffuse out of the  $\sim 2000^\circ\text{C}$  hot target and into a  $\sim 2000^\circ\text{C}$  tantalum ioniser. Cumulative  $^{152}\text{Tb}$  yields were significantly boosted by resonant laser ionisation of the radioactive precursor  $^{152}\text{Dy}$  (Köster, 2002). Following acceleration to 30 keV the ions were mass-separated by deflection in a magnetic dipole, and the  $A = 152$  ions were implanted into a pair of Al foils for gamma–gamma spectroscopy as well as a further metallised Mylar foil for electron–gamma spectroscopy. After decay of  $^{152}\text{Dy}$  to  $^{152}\text{Tb}$ , the samples were delivered to ILL. The first measurement began  $\sim 40$  h after collection at CERN. By this time, the small  $^{152\text{m}}\text{Eu}$  ( $T_{1/2} = 9.3116$  h (Martin, 2013)) admixture had decayed to  $< 1\%$  relative to  $^{152}\text{Tb}$  (Collins et al., 2023). The activities of the two Al-backed sources were approximately  $1 \times 10^5$  Bq and  $5 \times 10^5$  Bq at a reference time of 12:00 EST on 3rd May 2023, the first day of the experiment, estimated from the intensity of the 344-keV transition measured in later runs.

Gamma–gamma coincidence spectroscopy of the pair of decaying Al-backed sources was performed using the Fission Product Prompt  $\gamma$ -ray Spectrometer (FIPPS), an array of 64 HPGe detectors arranged

into 16 clovers (Michelagnoli et al., 2018; Cieplicka-Oryńczak et al., 2020). The clover configuration consists of four HPGe crystals encased in a bismuth germanate (BGO) Compton suppression shield. Of the 64 detectors, 14 were excluded from the current data analysis due to signal losses and distortions in the data. With this reduced configuration, the absolute full-energy peak efficiency of the array has been estimated to be approximately 9% at 344 keV using the coincidence counting method applied to a  $^{152}\text{Eu}$  calibration source (Collins et al., 2018). The preliminary efficiency curve is shown in Fig. 1, with gamma rays emitted in the decay of  $^{152}\text{Tb}$  shown for comparison. The final efficiency curve will be extended to higher energies using Monte Carlo simulations paired with previously known transitions in the decay of  $^{152}\text{Tb}$ .

A parallel electron–gamma spectroscopy experiment was carried out using the Mylar-backed third  $^{152}\text{Tb}$  source from the same ISOLDE production run. Measurements were taken using the LOHENGRIN/PN1 conversion electron spectroscopy setup at ILL, consisting of an HPGe clover paired with two lithium-drifted silicon (Si(Li)) detectors. Preliminary results from this parallel experiment will be presented in a subsequent paper (O'Sullivan et al., 2025).

## 3. Data analysis

Gamma-ray data were collected from FIPPS in singles mode, with a 120 ns coincidence window applied in off-line analysis. A total of seven days of data were collected between three source configurations: each of the two sources separately, followed by both together. After Compton suppression and HPGe clover detector addback,  $9.6 \times 10^9$  single events were collected from the higher activity source of the pair. Data from the lower activity source and from the combined sources are still being processed to correct for gain drift between and during runs. The energy calibration was carried out using a  $^{152}\text{Eu}$  source, the  $\beta^-$  decay of which shares the same  $^{152}\text{Gd}$  daughter as  $^{152}\text{Tb}$ , combined with a self-calibration using previously known transitions in the  $^{152}\text{Tb}$  decay up to energies of 3479 keV.

Several contaminants have been identified in the singles spectra. Runs at the beginning and end of the experimental period were examined to highlight those contaminants with lifetimes differing from  $^{152}\text{Tb}$ . These consist of several isobaric ( $^{152\text{m}}\text{Eu}$ ,  $^{152}\text{Eu}$ ) or near-isobaric ( $^{151}\text{Tb}$ ,  $^{152}\text{Tb}$ ,  $^{153}\text{Gd}$ ) species, as well as quasi-isobars which form molecules with  $M = 152$  ( $^{133}\text{Ba}$ ,  $^{133\text{m}}\text{Ba}$ ,  $^{134}\text{Ce/La}$ ), which may pass through the mass separator. All contaminants detected have activities less than 0.3% relative to the  $^{152}\text{Tb}$  activity. The activities of these contaminants, as well as upper limits on other possible undetected contaminants seen in similar production runs, will be calculated once the appropriate efficiency corrections have been established.

An energy-dependent time cut was applied to the gamma–gamma coincidence matrix, narrowing the coincidence window width to 40 ns for  $E_\gamma > 800$  keV to select for only prompt coincident gamma rays. A time random background was sampled using the same time gate offset by 120 ns, and subtracted from the coincidence data to remove chance coincident events. This resulted in  $3.3 \times 10^9$  coincident events from the higher activity of the two sources.

Gamma–gamma coincidence analysis was the primary method used to identify and place transitions on the level scheme. Coincidence spectra were produced by gating the coincidence matrix on a gamma-ray peak and subtracting a Compton background. Gating “from below” was used to investigate low-intensity gamma rays resulting from the decay of high-energy states in the daughter nucleus, the most likely states to have remained unidentified in previous studies. By gating on high-intensity transitions depopulating low energy states in  $^{152}\text{Gd}$ , these high-energy transitions can be revealed where they may otherwise have too low an intensity to be clearly visible in the singles spectrum. The placement of these transitions can be validated by reversing the gating, and examining the other transitions that appear in the same deexcitation cascade.

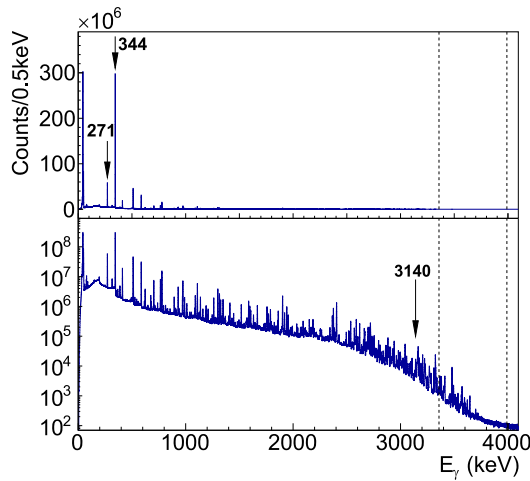


Fig. 2. Spectra showing singles events collected from 48 h of measurement of the higher activity source using FIPPS, on linear (top) and logarithmic (bottom) scales. The  $Q_{EC}$  value is marked at 3990 keV, along with the highest energy gamma ray placed in the previous study (3140 keV) and the highest energy level previously identified (3358 keV) (Martin, 2013). The two most intense gamma rays, at 344 keV and 271 keV, are marked on the top spectrum.

Spins were assigned to energy levels using angular correlation analysis, made possible by the FIPPS array geometry (Knafla et al., 2022). The detectors were considered clover-by-clover to increase the statistics available at each data point, giving a total of six possible angles between detector pairs. Since the array consists of two different HPGe clover types, the FIPPS and IFIN clovers, three different detector pairings are possible each with different corrections for the pair efficiency. As a result three different angular correlation distributions are produced, with a simultaneous minimisation performed across the three distributions to fit the overall angular correlation function for the cascade.

#### 4. Results

The preliminary spectra from the higher activity source indicate many previously unidentified peaks in the decay. All excited state and gamma-ray energies are reported to the nearest keV in these preliminary results. The singles spectrum in Fig. 2 marks the previous highest energy identified transition at 3140 keV, with many further peaks clearly visible at higher energies. The highest energy state identified in evaluated data is also shown at 3358 keV, again with many peaks visible above this energy. These support the suggestion of further high-energy states populated in  $^{152}\text{Gd}$  following the decay of  $^{152}\text{Tb}$ , previously unreported due to the limited efficiency of setups used in previous experiments compared to FIPPS.

The presence of strong peaks close to the  $Q_{EC}$  value suggests a comprehensive level scheme can be constructed from this dataset, especially with the use of gamma–gamma coincidence analysis to identify low-intensity peaks. While the pandemonium effect still limits this experiment in its ability to precisely measure the intensity of weak transitions, the expanded level scheme will allow for complementary techniques such as TAS to correct for this systematic error.

Preliminary gamma–gamma coincidence analysis primarily focused on the 344-keV gate; this is the most intense gamma ray emitted in the decay, and its decay directly to the ground state reduces the complexity of the cascades seen in these spectra. Gates on the 344-keV  $2^+ \rightarrow 0^+$  and 271-keV  $0^+ \rightarrow 2^+$  transitions are shown in Fig. 3. The singles spectrum is also shown for comparison; the  $Q_{EC}$  value of 3990 keV is marked, offset in each gate by the excitation energy of the depopulated state (344 keV and 615 keV for the 344-keV and 271-keV transitions respectively). Both gates show peaks close in energy to this upper

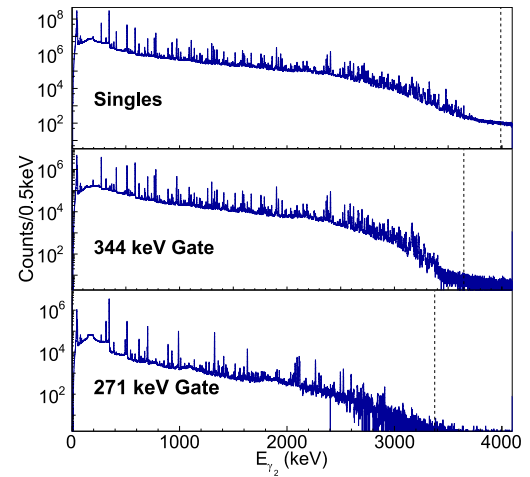


Fig. 3. Spectra showing single events, and coincident events gated on the 344-keV and 271-keV transitions in  $^{152}\text{Gd}$ . These data were collected from 48 h of measurement of the higher activity source using FIPPS. The  $Q_{EC}$  value is marked, with an offset in each gate corresponding to the energy of the depopulated state ( $E_i = 344$  keV for the 344-keV transition, and  $E_i = 615$  keV for the 271-keV transition).

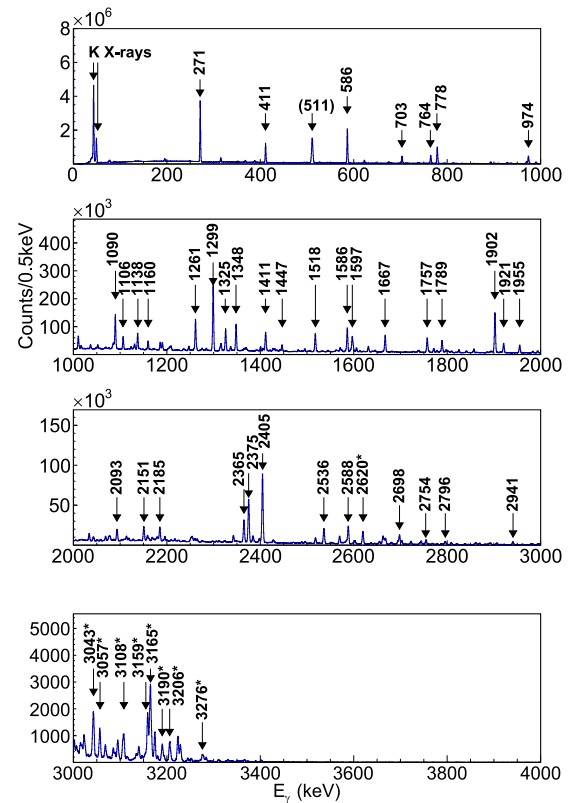


Fig. 4. Spectra showing the coincidence gate placed on the 344-keV transition, with a selection of prominent peaks labelled with transition energy in keV. K-shell x-rays and the 511-keV annihilation peak are also marked on the spectra. Labels marked with an asterisk are not in the evaluated data (Martin, 2013).

limit, with the lack of peaks seen above these limits demonstrating the effectiveness of the Compton background subtraction and the prompt time cut in limiting the presence of chance coincidences in the gates.

A more detailed view of the 344-keV coincidence gate is given in Fig. 4, with a selection of 47 prominent peaks marked. Of the labelled peaks nine are not in the most recently evaluated decay data, and their presence in these spectra indicate that these transitions occur

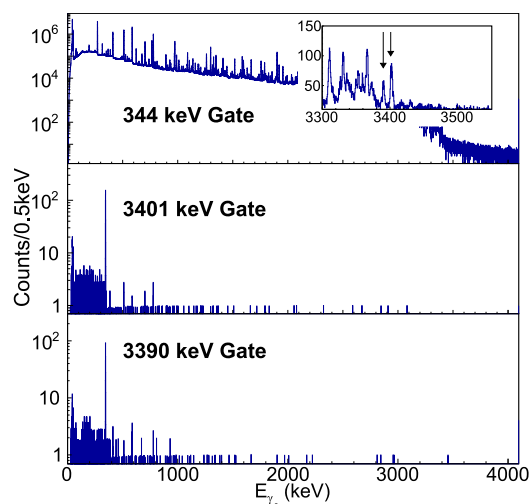


Fig. 5. Spectra showing coincidence gates placed on the 344-keV, 3401-keV, and 3390-keV transitions. The inset on the 344-keV spectrum magnifies the high-energy end of the scale, with the 3401-keV and 3390-keV peaks marked.

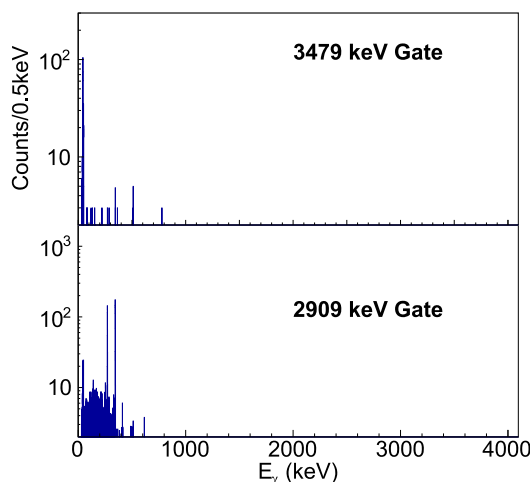


Fig. 6. Spectra showing coincidence gates placed on the 3479-keV and 2909-keV transitions.

as parts of various deexcitation cascades to the 344-keV level. By examining which other coincidence gates these transitions appear in, as well as reversing the gating where possible, the initial and final states of each transition may be found.

High energy peaks observed in the 344-keV  $2^+ \rightarrow 0^+$  gate are likely to decay directly to the 344-keV state, with no intermediate decay channels available for transitions at energies greater than 3375-keV (the energy difference between the  $Q_{EC}$  value and the 615-keV state). Fig. 5 shows two previously unplaced high-energy transitions identified in the 344-keV gate at 3401 keV and 3390 keV. The placement of these transitions is verified by reversing the gating, showing only the 344-keV transition and Gd K-shell x-rays ( $K\alpha_1 = 43$  keV) visible in these cascades. The origin of these gamma rays are previously unidentified high-energy states at 3746 keV and 3735 keV respectively.

Further examples of gamma-gamma coincidence analysis are demonstrated in Fig. 6, showing gates on the 3479-keV and 2909-keV gamma rays. The 3479-keV gate shows no other gamma rays in coincidence with this transition, only x-rays originating from the electron capture, demonstrating that this transition is the result of the newly identified 3479-keV state decaying directly to the ground state. Both the 344-keV and the 271-keV gamma rays are visible in the 2909-keV gate,

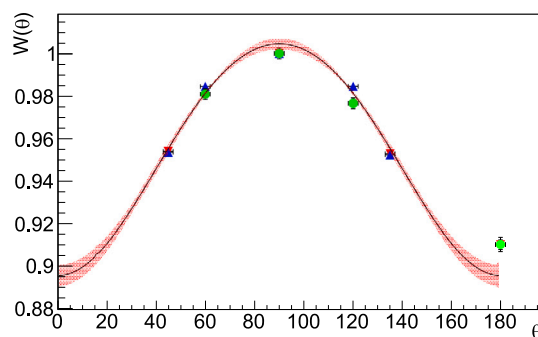


Fig. 7. Angular correlation function produced by gating on the 344-keV and 778-keV transitions in the  $^{152}\text{Eu}$  calibration source, taken from 7 days of measurement with FIPPS. Data points from each clover combination are shown, with FIPPS-FIPPS in red, FIPPS-IFIN in blue, and IFIN-IFIN in green.

suggesting that this gamma ray populates the 615-keV state which subsequently decays to the 344-keV state. This indicates that the origin of the 2909-keV transition is the newly identified 3524-keV state.

Angular correlations are used to assign spins to energy states populated in the decay, based on the distribution of intensity of a coincident pair of gamma rays with angle. Fig. 7 demonstrates this using the  $^{152}\text{Eu}$  calibration source, which populates the same  $^{152}\text{Gd}$  daughter as  $^{152}\text{Tb}$ . The normalised intensity of the 344-keV and 778-keV coincident pair is shown at different angles, using the three possible clover pairings to fit the overall angular correlation function  $W(\theta)$ . The resulting distribution matches the expected shape for a cascade of this type: spin/parity  $3^- \rightarrow 2^+ \rightarrow 0^+$ .

Further possible angular correlation functions are illustrated in Fig. 8, taken from the decay of the  $^{152}\text{Tb}$  source. Each distribution matches the expected shape, showing cascades of spin  $0 \rightarrow 2 \rightarrow 0$ ,  $4 \rightarrow 2 \rightarrow 0$ , and  $3 \rightarrow 2 \rightarrow 0$  respectively.

The assignment of spin to a previously unreported state in  $^{152}\text{Gd}$  is shown in Fig. 9. The known  $2 \rightarrow 2 \rightarrow 0$  cascade, consisting of the 1299-keV and 344-keV transitions, is compared to the cascade depopulating the newly identified 3567-keV state, consisting of the 3223-keV and 344-keV transitions. The function shapes match, suggesting a spin 2 assignment to the 3567-keV state.

Angular correlations alone are not sufficient to assign parity to the state, although a negative parity is suggested from the  $E1/M2$  multipolarity mixing that produces this function shape. While a  $2^-$  spin and parity is most probable, as allowed beta decays from the  $^{152}\text{Tb}$   $J^\pi = 2^-$  ground state populate only negative parity states in  $^{152}\text{Gd}$ , further evidence is required to support this assignment. The parity of this state determines the multipolarity, and thereby the intensity, of the transition to the  $J^\pi = 0^+$  ground state: a  $2^+$  to  $0^+$  transition must have multipolarity  $E2$ , while a  $2^-$  to  $0^+$  transition must have an  $M2$  multipolarity. Since magnetic transitions have a much lower probability than electric transitions of the same order, we would expect to see this ground state transition prominently only in the case of a  $2^+$  state decaying. As there is no transition observed at this energy, we can assign a  $2^-$  spin and parity to the 3567-keV state.

## 5. Discussion

The placement of transitions to five previously unreported states have been demonstrated, including the spin and parity assignment of the 3567-keV state. All five are at energies greater than any excited state previously identified, with the 3745-keV state at almost 400 keV above the previous maximum energy level. Intensities are not reported for these gamma-ray transitions in the current work, but will be presented in a future publication when corrections for detector efficiency, summation effects, and radioactive background have been finalised.



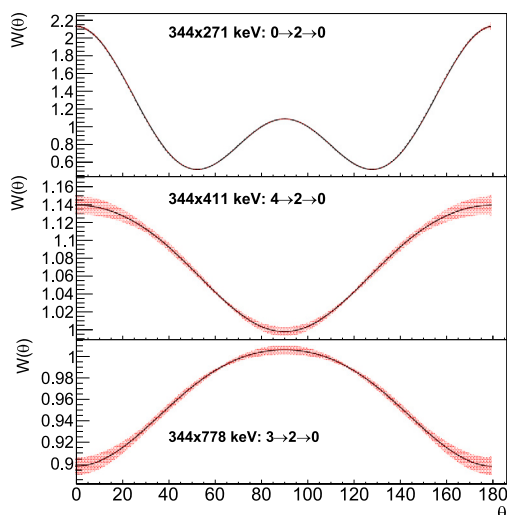


**Fig. 8.** Angular correlation functions produced by gating the 344-keV transition with the 271-keV (top), 411-keV (middle), and 778-keV (bottom) transitions in the higher activity  $^{152}\text{Tb}$  source using FIPPS. The spins of the states involved in each cascade are marked (Martin, 2013).

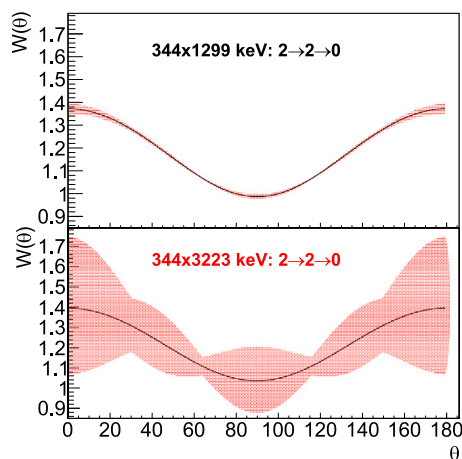
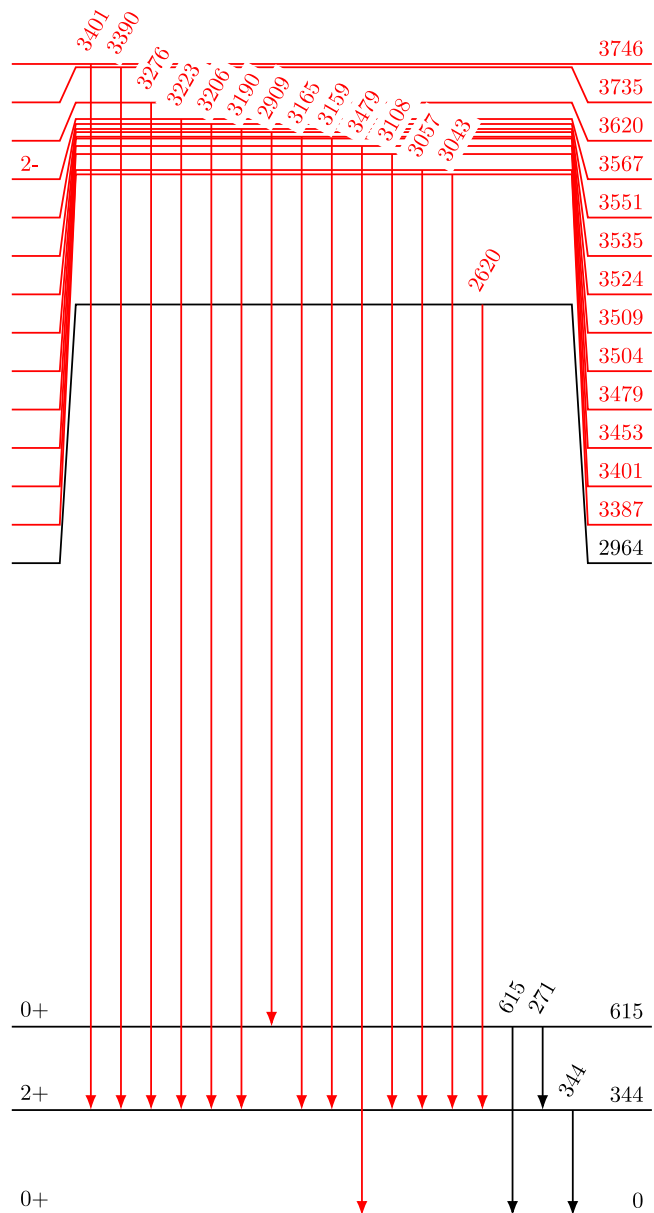


Fig. 9. Angular correlation functions produced by gating the 344-keV transition with the 1299-keV (top) and 3223-keV (bottom) transitions in the higher activity  $^{152}\text{Tb}$  source using FIPPS. The spins of the states involved in each cascade are marked (Martin, 2013), with the new spin assignment for the 3567-keV state given in red.

The transitions reported here range in intensity from approximately 0.09% to 0.001% relative to the 344-keV transition, as measured in the 344-keV coincidence gate by comparison to the 586-keV gamma ray. The finalised intensities, calculated from measured peak areas in the gamma–gamma coincidence spectra, will be vital in calculating the feeding into and out of each level, and thereby the beta decay strength.

Nine prominent unplaced transitions are presented in coincidence with the 344-keV gamma ray, some of which confirm unpublished identifications of high-energy states in  $^{152}\text{Gd}$  (Beller, 2014). In particular the placements of the 3156-keV and 3159-keV transitions confirm those proposed by Beller, with the 3401-keV, 3057-keV, 3043-keV, and 2620-keV gamma rays also within 1 keV of similarly placed transitions given in the thesis. Beller also reports transition energies to the nearest keV and without intensities, and as such the continued analysis of these data will further develop the results achieved in the 2014 study.

A further eight excited states are presented following coincidence analysis of these nine transitions (see Fig. 10). This demonstrates that gamma-gamma coincidence analysis of these data has potential to confirm the existence and identify the position of many of the 248



**Fig. 10.** Partial level scheme for the decay of  $^{152}\text{Tb}$  into  $^{152}\text{Gd}$ , showing a selection of energy levels identified in the 344-keV coincidence gate. Levels marked in red have not been previously reported in published work, and transitions marked in red have not been placed in evaluated data.

unplaced transitions noted in the evaluated data to the level scheme, in addition to the identification of previously unidentified transitions and excited states. The density of gamma rays seen in these spectra support the suggestion that many further levels may be identified from these data, representing a significant change to the beta decay strength function and therefore the dose received by patients.

Electron-gamma measurements using the LOHENGRIN/PN1 conversion electron spectrometer will further support the construction of the level scheme by measuring E0 transitions and internal conversion. These represent further transition intensity that is invisible to HPGe detectors, and is not present on gamma-ray spectra. Furthermore, electron emission represents a significant contribution to the dose received by patients due to the near-complete deposition of energy in the patient's body compared to gamma rays. Internal conversion coefficients can also be used to infer the multipolarity of transitions, further supporting the spin and parity assignments from gamma-gamma coincidence data.

## 6. Conclusion

Thirteen newly identified excited states are reported in  $^{152}\text{Gd}$ , populated following the decay of  $^{152}\text{Tb}$ . These are based on the new placement of fourteen gamma-ray transitions following gamma–gamma coincidence analysis. The spin and parity of one of these states has been assigned following angular correlation analysis of gamma rays emitted in the deexcitation cascade. Spectra are presented suggesting the existence of many further unidentified states, the analyses of which are in progress using the methods and data presented here. The addition of further high-energy states to the level scheme of this decay will have significant implications for the medical use of  $^{152}\text{Tb}$  in PET imaging, with the re-evaluated decay strength function to result in a revised gamma-ray and  $\beta^+$  dose to patients.

## CRediT authorship contribution statement

**E.B. O'Sullivan:** Writing – review & editing, Writing – original draft, Visualization, Software, Methodology, Investigation, Formal analysis. **S.M. Collins:** Writing – review & editing, Supervision, Methodology, Conceptualization. **J.-M. Daugas:** Methodology, Investigation, Conceptualization. **L. Domenichetti:** Software, Methodology. **J. Heery:** Writing – review & editing, Software, Methodology, Investigation, Formal analysis. **J. Henderson:** Supervision, Methodology, Funding acquisition. **U. Köster:** Writing – review & editing, Methodology, Investigation, Conceptualization. **C. Michelagnoli:** Writing – review & editing, Methodology, Investigation, Conceptualization. **T. Parry:** Software. **S. Pascu:** Writing – review & editing, Methodology, Investigation. **P.H. Regan:** Writing – review & editing, Supervision, Project administration, Methodology, Investigation, Funding acquisition, Conceptualization. **R. Shearman:** Writing – review & editing, Supervision, Methodology, Investigation, Conceptualization.

## Declaration of competing interest

The authors declare that they have no known competing financial interests or personal relationships that could have appeared to influence the work reported in this paper.

## Acknowledgements

E.B.O'S acknowledges funding via a PhD scholarship bursary from the UK EPSRC. The work performed at NPL was supported by the National Measurements System Programmes Unit of the UK's Department for Science, Innovation and Technology, and the European Union's Horizon 2020 research and innovation programme under grant agreement No 101008571 (PRISMAP — The European medical radionuclides programme). P.H.R also acknowledges funding from the UK Science and Technologies Facilities Council under grant numbers ST/P005314/1, ST/V001108/1, ST/L005743/1 and ST/P005314. Thank you to the CERN-ISOLDE teams, including target, RILIS, operations, and RP.

## Data availability

Data will be made available on request.

## References

- Adam, J., Dobeš, J., Honusek, M., Kalinnikov, V.G., Mrázek, J., Pronskikh, V.S., Čaloun, P., Lebedev, N.A., Stegailov, V.I., Tsoukko-Sitnikov, V.M., 2003. Properties of  $^{152}\text{Gd}$  collective states. *Eur. Phys. J. A* 18 (4), 605–626. <http://dx.doi.org/10.1140/epja/i2002-10167-8>.
- Baum, R.P., Singh, A., Benešová, M., Vermeulen, C., Gnesin, S., Köster, U., Johnston, K., Müller, D., Senftleben, S., Kulkarni, H.R., Türler, A., Schibli, R., Prior, J.O., van der Meulen, N.P., Müller, C., 2017. Clinical evaluation of the radiolanthanide terbium-152: first-in-human PET/CT with  $^{152}\text{Tb}$ -DOTATOC. *Dalton Trans.* 46 (42), 14638–14646. <http://dx.doi.org/10.1039/c7dt01936j>.
- Beller, J., 2014. Systematische Untersuchung exotischer Zerfallskanäle der Scherenmode in Gadoliniumisotopen.
- Capote, R., Herman, M., Obložinský, P., Young, P., Goriely, S., Belgia, T., Ignatyuk, A., Koning, A., Hilaire, S., Plujko, V., Avrigeanu, M., Bersillon, O., Chadwick, M., Fukahori, T., Ge, Z., Han, Y., Kailas, S., Kopecky, J., Maslov, V., Reffo, G., Sin, M., Soukhovitskii, E., Talou, P., 2009. RIPL — Reference input parameter library for calculation of nuclear reactions and nuclear data evaluations. *Nucl. Data Sheets* 110 (12), 3107–3214. <http://dx.doi.org/10.1016/j.nds.2009.10.004>.
- Cieplicka-Oryńczak, N., Michelagnoli, C., Gargano, A., Fornal, B., Leoni, S., Benzoni, G., Blanc, A., Bottoni, S., Crespi, F.C.L., Iskra, L.W., Jentschel, M., Köster, U., Mutti, P., Pietralla, N., Ruiz-Martinez, E., Werner, V., 2020. Contrasting properties of particle-particle and hole-hole excitations in  $^{206}\text{Tl}$  and  $^{210}\text{Bi}$  nuclei. *Phys. Lett. B* 802, 135222. <http://dx.doi.org/10.1016/j.physletb.2020.135222>.
- Collins, S.M., Köster, U., Robinson, A.P., Ivanov, P., Cocolios, T.E., Russell, B., Fenwick, A.J., Bernerd, C., Stegemann, S., Johnston, K., Gerami, A.M., Chrysalidis, K., Mohamud, H., Ramirez, N., Bhaisare, A., Mewburn-Crook, J., Cullen, D.M., Pietras, B., Pells, S., Dockx, K., Stucki, N., Regan, P.H., 2023. Determination of the Terbium-152 half-life from mass-separated samples from CERN-ISOLDE and assessment of the radionuclide purity. *Appl. Radiat. Isot.* 202, 111044. <http://dx.doi.org/10.1016/j.apradiso.2023.111044>.
- Collins, S., Shearman, R., Keightley, J., Regan, P., 2018. Investigation of  $\gamma - \gamma$  coincidence counting using the National Nuclear Array (NANA) as a primary standard. *Appl. Radiat. Isot.* 134, 290–296. <http://dx.doi.org/10.1016/j.apradiso.2017.07.056>.
- Gomes Marin, J.F., Nunes, R.F., Coutinho, A.M., Zaniboni, E.C., Costa, L.B., Barbosa, F.G., Queiroz, M.A., Cerri, G.G., Buchpiguel, C.A., 2020. Theranostics in nuclear medicine: Emerging and re-emerging integrated imaging and therapies in the era of precision oncology. *RadioGraphics* 40 (6), 1715–1740. <http://dx.doi.org/10.1148/rq.2020200021>.
- Gula, A.C., McCutchan, E.A., Lister, C.J., Greene, J.P., Zhu, S., Ellison, P.A., Nickles, R.J., Carpenter, M.P., Smith, S.V., Sonzogni, A.A., 2020. State-of-the-art  $\gamma$ -ray assay of  $^{86}\text{Y}$  for medical imaging. *Phys. Rev. C* 102 (3), <http://dx.doi.org/10.1103/physrevc.102.034316>.
- Hardy, J.C., Carraz, L.C., Jonson, B., Hansen, P., 1977. The essential decay of pandemonium: A demonstration of errors in complex beta-decay schemes. *Phys. Lett. B* 71 (2), 307–310. [http://dx.doi.org/10.1016/0370-2693\(77\)90223-4](http://dx.doi.org/10.1016/0370-2693(77)90223-4).
- Knafla, L., Esmaylzadeh, A., Harter, A., Jolie, J., Köster, U., Ley, M., Michelagnoli, C., Régis, J.-M., 2022. Development of a new  $\gamma$ - $\gamma$  angular correlation analysis method using a symmetric ring of clover detectors. *Nucl. Instrum. Methods Phys. Res. Sect. A: Accel. Spectrometers, Detect. Assoc. Equip.* 1042, 167463. <http://dx.doi.org/10.1016/j.nima.2022.167463>.
- Köster, U., 2002. Resonance ionization laser ion sources. *Nucl. Phys. A* 701 (1–4), 441–451. [http://dx.doi.org/10.1016/S0375-9474\(01\)01625-6](http://dx.doi.org/10.1016/S0375-9474(01)01625-6).
- Martin, M., 2013. Nuclear data sheets for  $A = 152$ . *Nucl. Data Sheets* 114 (11), 1497–1847. <http://dx.doi.org/10.1016/j.nds.2013.11.001>.
- Michelagnoli, C., Blanc, A., Ruiz-Martinez, E., Chebboubi, A., Faust, H., Froidefond, E., Kessedjian, G., Jentschel, M., Köster, U., Mutti, P., Simpson, G., 2018. FIPPS (Fission product prompt  $\gamma$ -ray spectrometer) and its first experimental campaign. In: Köster, U. (Ed.), *EPJ Web Conf.* 193, 04009. <http://dx.doi.org/10.1051/epjconf/201819304009>.
- Müller, C., Domnanich, K.A., Umbricht, C.A., van der Meulen, N.P., 2018. Scandium and terbium radionuclides for radiotheranostics: current state of development towards clinical application. *Br. J. Radiol.* 91 (1091), 20180074. <http://dx.doi.org/10.1259/bjr.20180074>.
- Müller, C., Singh, A., Umbricht, C.A., Kulkarni, H.R., Johnston, K., Benešová, M., Senftleben, S., Müller, D., Vermeulen, C., Schibli, R., Köster, U., van der Meulen, N.P., Baum, R.P., 2019. Preclinical investigations and first-in-human application of  $^{152}\text{Tb}$ -PSMA-617 for PET/CT imaging of prostate cancer. *EJNMMI Res.* 9 (1), <http://dx.doi.org/10.1186/s13550-019-0538-1>.
- Nichols, A.L., 2022. Status of the decay data for medical radionuclides: existing and potential diagnostic  $\gamma$  emitters, diagnostic  $\beta^+$  emitters and therapeutic radioisotopes. *Radiochim. Acta* 110 (6–9), 609–644. <http://dx.doi.org/10.1515/ract-2022-0004>.
- O'Sullivan, E.B., Collins, S.M., Daugas, J.-M., Domenichetti, L., Heery, J., Henderson, J., Köster, U., Michelagnoli, C., Parry, T., Pascu, S., Regan, P.H., Shearman, R., 2025. Electron-Gamma decay spectroscopy of  $^{152}\text{Tb}$ . *Phys. Scr.* (submitted for publication).
- Rubio, B., Gelletly, W., Algara, A., Nacher, E., Tain, J.L., 2017. Beta decay studies with total absorption spectroscopy and the Lucrecia spectrometer at ISOLDE. *J. Phys. G: Nucl. Part. Phys.* 44 (8), 084004. <http://dx.doi.org/10.1088/1361-6471/aa797f>.